Chemical Science

ROYAL SOCIETY OF CHEMISTRY

EDGE ARTICLE

View Article Online
View Journal

Cite this: DOI: 10.1039/d6sc01682k

All publication charges for this article have been paid for by the Royal Society of Chemistry

Turn-on fluorescence switching and radical formation in a dual-functional negative photochromic dimethyldihydropyrene

Sariful Molla, [a] Samyadeb Mahato, [ab] Avinash Kumar Ray[a] and Subhajit Bandyopadhyay *[a]

High-contrast fluorescent switchable systems are highly coveted dyes for bioimaging. Here, we report a molecular system that integrates reversible fluorescence modulation and radical formation in a series of covalently linked triphenylamine (TPA)–dimethyldihydropyrene (DHP) photochromic systems. DHP units with different substitutions directly alter the electron density of the photochromic unit, thereby regulating electronic communication with TPA. Photoinduced ring opening of the DHP core activates a charge transfer pathway, resulting in a dramatic enhancement of fluorescence, as reflected in the enhancement of quantum yield from 0.01 to 0.31. The emission can be reversibly turned off by ultraviolet irradiation or heating. Importantly, the bright state is accessed using visible light, making this negative photochromic system particularly attractive for bioimaging applications. Beyond emission control, irradiation of the same molecule at 370 nm in chloroform generates a long-lived radical. The coexistence of controlled fluorescence switching and radical formation highlights the potential of this design strategy to create multifunctional molecular systems. Such bifunctional platforms open new opportunities for accessing optical readout and chemical activity on demand within a single molecular scaffold.

Received 27th February 2026
Accepted 27th April 2026

DOI: 10.1039/d6sc01682k

rsc.li/chemical-science

Introduction

Due to their applications in the rapid detection of intracellular species, bioimaging, and optical and memory devices, fluorescent materials have attracted considerable attention over the past decade.[1–7] Despite the presence of numerous methods for fluorescent imaging, tracking of analytes is often challenging due to background interference, which further complicates identification.[8] In this regard, fluorescent probes coupled with photochromic molecules offer excellent improvements.[9–15] These systems are capable of reversibly shifting fluorescence between ON and OFF states upon exposure to different light sources within *in situ* biological environments.[16–20] Therefore, unwanted background signals can be minimized using the double-check method *via in situ* reversible photoisomerization between the two states. Another interesting potential application of photoswitchable fluorescent materials is single-molecule labelling and super-resolution imaging.[21] Such imaging techniques offer higher resolution by turning them OFF and ON for recording and distinguishing them from the background.[22] Therefore, photoswitchable molecules offer excellent options for the next generation of super-resolution imaging techniques. These photoswitchable fluorescent systems should possess: (a) high contrast of the on/off states, (b) thermal and photostability of both isomers and (c) high photoconversion.[21] Innovative advancements have been achieved using reversibly photoswitchable fluorescent dyes facilitated by photochromic molecules.[23–26] Among these systems, "turn-off" mode fluorescence switches are prevalent, in which the initial state exhibits fluorescence and the photogenerated coloured state is non-fluorescent,[27–29] and are used in optical memory devices and RESOLFT-type super-resolution microscopy.[30] In contrast, "turn-on" mode fluorescence switching finds applications in super-resolution imaging using photoactivated localization microscopy (PALM) and stochastic optical reconstruction microscopy (STORM) techniques.[31] To this end, "turn-on" mode fluorescence switching with positive photochromic molecules, such as diarylethenes or spirooxazine derivatives, was achieved by Irie and Raymo.[32,33] Recently, Hell and coworkers used turn-on type fluorescence switching in diarylethenes for bioimaging and single-molecule localization microscopy.[21] Upon switching, if the thermally stable, less colored or colorless isomer generates a colored isomer, it falls under the category of positive photochromic systems.[34–38] However, 'turn on' type fluorescence switching in positive photochromic systems, where the stable colorless isomer generates a colored isomer, has certain disadvantages, particularly because of the screening effect and

[a]*Department of Chemical Sciences, Indian Institute of Science Education and Research Kolkata, 741246 Mohanpur, Nadia, WB, India. E-mail: sb1@iiserkol.ac.in*

[b]*Department of Chemistry, Simon Fraser University, Burnaby, British Columbia V5A 1S6, Canada*

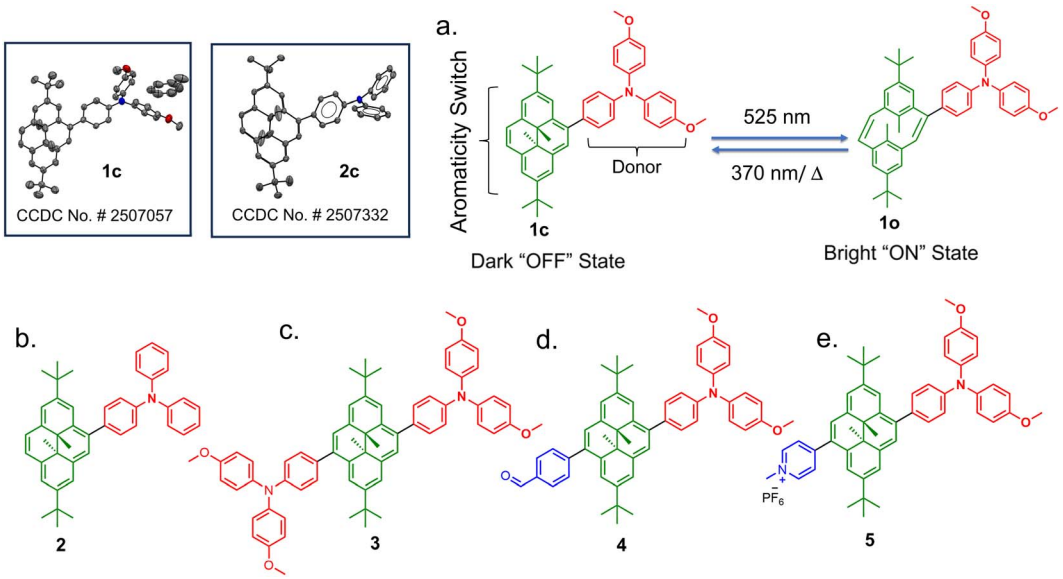

Fig. 1 (a) Light-induced isomerization between **1c**/**1o** and emission OFF/ON control. (b) Molecule with a comparatively lower electron-donating unit. (c) Two strong donor units. (d) Push–pull system having *para*-benzaldehyde as the acceptor. (e) Push–pull system having a pyridinium cation as the acceptor.

fluorescence quenching due to self-absorption; it can also cause photobleaching of the dye due to the use of high-energy UV light.[39,40] Negative photochromic systems that switch from a thermally stable colored state to a less-colored state using long wavelength light can offer a solution to these problems.[41–45] For *in vivo* imaging, this is important because UV light often causes cell damage. The decoloration upon switching minimizes the screening effect and helps maintain the photochromic efficiency of the system with high conversion to the other isomeric state.[46–48] In addition, for these "turn-on" type photoactivatable fluorescence switches, the colorless form possesses high fluorescence intensity by reducing the possibility of self-absorption. However, examples of reversible fluorescence switching mediated by negative photochromic molecules remain exceedingly scarce, underscoring the inherent challenges associated with achieving efficient emissive modulation in such systems. Herein, we report a DHP-based "turn-on" fluorescence switch, coupled with a strong donor, *para*-methoxy-triphenylamine (TPA). The negative photochromic DHP is a highly aromatic system; it acts as a π-switch as the photoisomeric cyclophanediene form (CPD) has a large difference in the electronic conjugation of the π-framework (Fig. 1a). When attached to the TPA moiety, despite its extended conjugation and planar geometry, the closed isomer does not exhibit any noticeable charge transfer band. In contrast, visible light-induced ring opening generates a charge transfer-driven emission band in the non-planar step-like open CPD isomer. Achieving stable radical cations under mild conditions remains a significant challenge, as most organic systems undergo rapid recombination or irreversible degradation following the oxidation.[49–51] Triphenylamine derivatives have emerged as a privileged molecular platform for stabilizing radical cations due to their propeller-like geometry and efficient delocalization of positive charge across multiple aromatic rings.[52–54] These characteristics suppress localized reactivity and extend radical lifetimes in solution and solid states. As a result, TPA-based radical cations have been widely exploited as hole transport materials and redox-active components in organic assemblies.[55–58] However, generation of radicals is most commonly achieved through electrochemical or chemical oxidation, which limits their spatial control and compatibility with biological applications.[59,60]

Light-driven formation of radical cations presents an attractive alternative, enabling remote, reversible, and localized activation within a molecular system.[61–63] Integrating photoresponsive units with redox-active donors provides a strategy to achieve such control while preserving molecular stability.[64–66] In this context, the DHP scaffold serves as a unique photochemical trigger that can regulate the electronic structure *via* reversible aromaticity switching. Coupling this unit with a triphenylamine donor allows direct access to a photogenerated radical cation state under irradiation in solution. The resulting system thus bridges photochromism and radical chemistry, offering a multifunctional platform relevant to both optoelectronic devices and super-resolution imaging.

Results and discussion

Derivatives **1** and **2** were synthesized by Suzuki–Miyaura C–C coupling of mono-bromo-dimethyldihydropyrene (DHP-Br) with the boronic acids of *p*-methoxy-triarylamine and triphenylamine, respectively (Schemes S1 and S2). Compound **3** was synthesized similarly using a coupling reaction between dibromo-dimethyldihydropyrene (DHP-Br_2) and the boronic acid of *p*-methoxy-triarylamine (Scheme S3). For derivatives **4** and **5**, a mono-bromo-mono-iodo-dimethyldihydropyrene (Br-DHP-I)

Table 1 Photophysical data of DHPs **1–5** in toluene

	λ_{abs} (nm)/ε (M^{-1} cm^{-1})					$\%_{PSS}$ at λ_{irr} (nm)		Φ_{iso} (10^{-3})	
	c				o				
DHPs	$S_0 \rightarrow S_1$	$S_0 \rightarrow S_2$	$S_0 \rightarrow S_3$	$S_0 \rightarrow S_4$	$S_0 \rightarrow S_1$	c : o (525)	o : c (370)	c → o	$t_{1/2}$ (h)
1	653/900	486/8700	398/41 000	346/57 000	371/28 400	>99 : 1	72 : 28	0.80	77
2	652/1100	486/9400	396/46 300	349/49 700	352/21 800	>99 : 1	71 : 29	1.65	38
3	661/8300	498/7600	415/37 600	344/28 500	367/30 600	>99 : 1	74 : 28	0.18	36
4	662/1900	496/12 700	413/47 900	348/45 800	352/36 600	>99 : 1	82 : 18	0.23	25
5	682/4000	562/11 100	441/24 900	346/42 200	389/20 200	>99 : 1	85 : 18	NA[a]	1

[a] The photoisomerization of compound **5** is too fast to determine Φ_{iso} with high accuracy.

molecule was synthesized, followed by similar coupling reactions that yielded the final compounds (Schemes S4 and S5). All the new compounds were thoroughly characterized by NMR spectroscopy (^1H and ^{13}C) and high-resolution mass spectrometry (Fig. 1a–e, see the SI for the details, Fig. S1 and S12). The compounds **1** and **2** were also characterized by single crystal X-ray analysis (CCDC no. 2507057 and 2507332, respectively; Fig. S40, S41 and Table S7). The photophysical measurements were performed in toluene unless otherwise stated (Table 1). We started by investigating light-induced isomerization in solution. All compounds exhibiting intense absorbance bands in both the UV and visible regions possess a deep color in their closed form. Initially, the green solution of **1** and **2** and the brownish-red solution of **3** and **4**, upon illumination with visible light (525 nm, 35 mW cm^{-2}), underwent electrocyclic ring-opening isomerization to the colorless CPD forms. The absorbance peaks of the DHP forms in the visible region gradually diminished as the CPD forms were generated (Fig. 2a and S13–S15). The cationic DHP form **5** displayed a red-shifted band in comparison to the neutral molecules, which enabled its long wavelength switching with both 740 nm NIR and 640 nm red light to the CPD form (Fig. S16). It was remarkable that all the compounds exhibited almost quantitative ring-opening photoisomerization (c → o) with

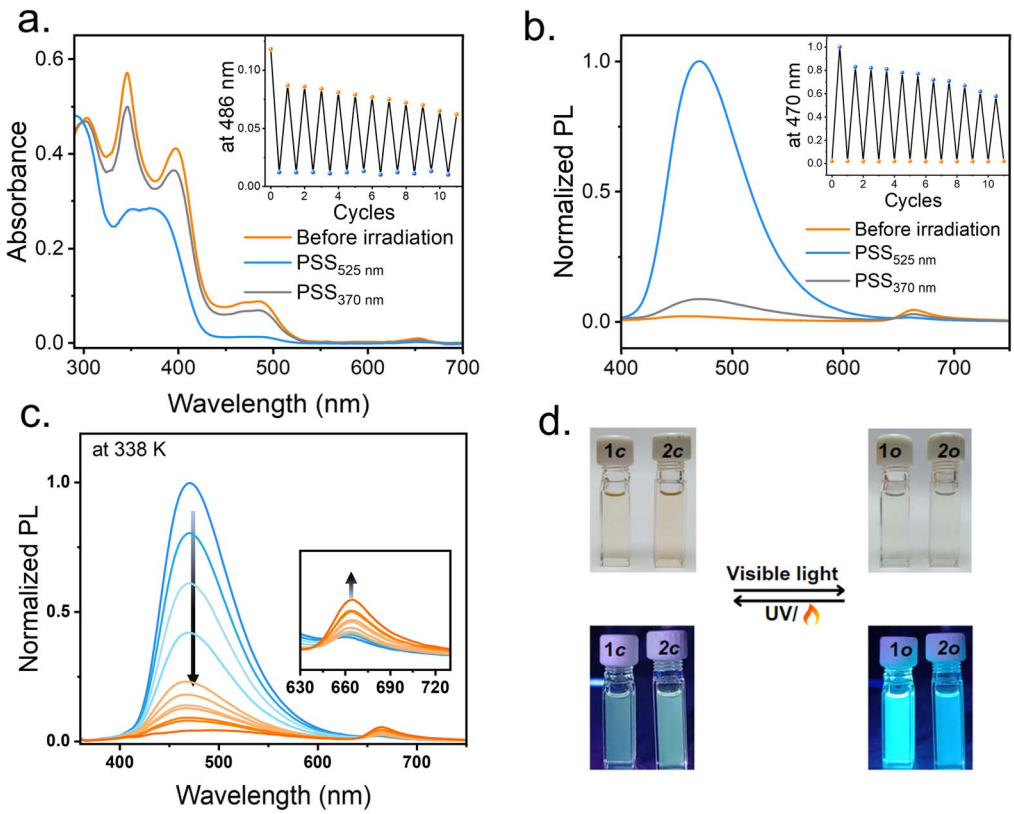

Fig. 2 (a) UV-vis absorption and (b) PL spectra of compound **1** in toluene solvent. The inset shows the switching cycles under alternating irradiation of 525 nm and 370 nm. (c) Reduction of PL intensity due to thermal reversal (**1o** → **1c**) at 338 K. (d) Images of "turn on" mode fluorescence switches **1** and **2**.

Table 2 Fluorescence properties of compounds **1–4**

	λ_{em} (nm)		Φ_{em} (%)		Brightness[a] (M^{-1} cm^{-1}) ($\times 10^3$)	
DHPs	c	o	c	o	c	o
1	664	470	1.02 ± 0.7	31.3 ± 0.5	0.54	8.83
2	662	446	1.13 ± 0.6	6.12 ± 0.6	0.69	3.27
3	678	471	0.85 ± 0.7	8.38 ± 0.6	0.23	2.25
4	678	488	0.21 ± 0.8	5.27 ± 0.6	0.09	1.93

[a] Brightness = $\varepsilon \times \Phi_{em}$. For **5**, the emission intensity is too weak to be accurately measured.

a photostationary state (PSS) of >99 : 1 (o : c). The photoisomerization quantum yields (Φ_{iso}, c → o) have been presented in Table 1. The reverse photoisomerization (o → c) could be achieved by 370 nm light (35 mW cm^{-2}) for compounds **1–4** and 456 nm (35 mW cm^{-2}) for **5**. Thus, derivative **5** is an all-visible light-enabled photoswitch, where back-and-forth switching can be performed without the use of UV light in cycles (Fig. S16). The PSS of the reverse isomerization (o → c) was found to be 71–74% for compounds **1–3** and 82–85% for **4** and **5**. All the PSS compositions were calculated by using ^{1}H-NMR spectroscopy (Fig. S28–S32); for example, in compound **1**, the internal methyl protons appear around δ −3.5 due to the high diamagnetic anisotropic effect of the 14π aromatic DHP ring current which upon ring opening (**1c** → **1o**) shifts to δ +2.2 suggesting breaking of the planar aromatic ring to a step-like molecule with two discrete 6π-electronic aromatic systems (Fig. S28). The ring opening (c → o) photoisomerization quantum yield Φ_{iso} was investigated; however, the ring closing photoisomerization (o → c) was too fast to allow the measurement of the Φ_{iso} accurately (Tables 1, S2 and Fig. S33). The thermal stability of the photo-generated CPD isomers was studied by variable-temperature UV-vis studies. The Arrhenius and Eyring plots thus obtained gave the thermodynamic parameters for the thermal closing of the derivatives (Fig. S18–S27). The open CPD isomers of **1–5** have half-lives spanning from 1 to 77 h at 298 K (Tables 1 and S1), providing high tunability of the thermal reversal of the ring-opened isomers.

The photoluminescence emission measurements show that all the compounds exhibit a characteristic PL band at approximately 680 nm, attributed to the presence of DHP as a chromophore unit (Fig. 2b and S13–S16). While investigating the isomerization process by PL spectroscopy, an interesting phenomenon was observed: the ring-opening (c → o) of DHP derivatives (**1–5**) results in a distinct growth of a strong PL band around ~470 nm (blue line, Fig. 2b). This emissive state can be reversibly switched off by exposure to UV light (370 nm) (grey

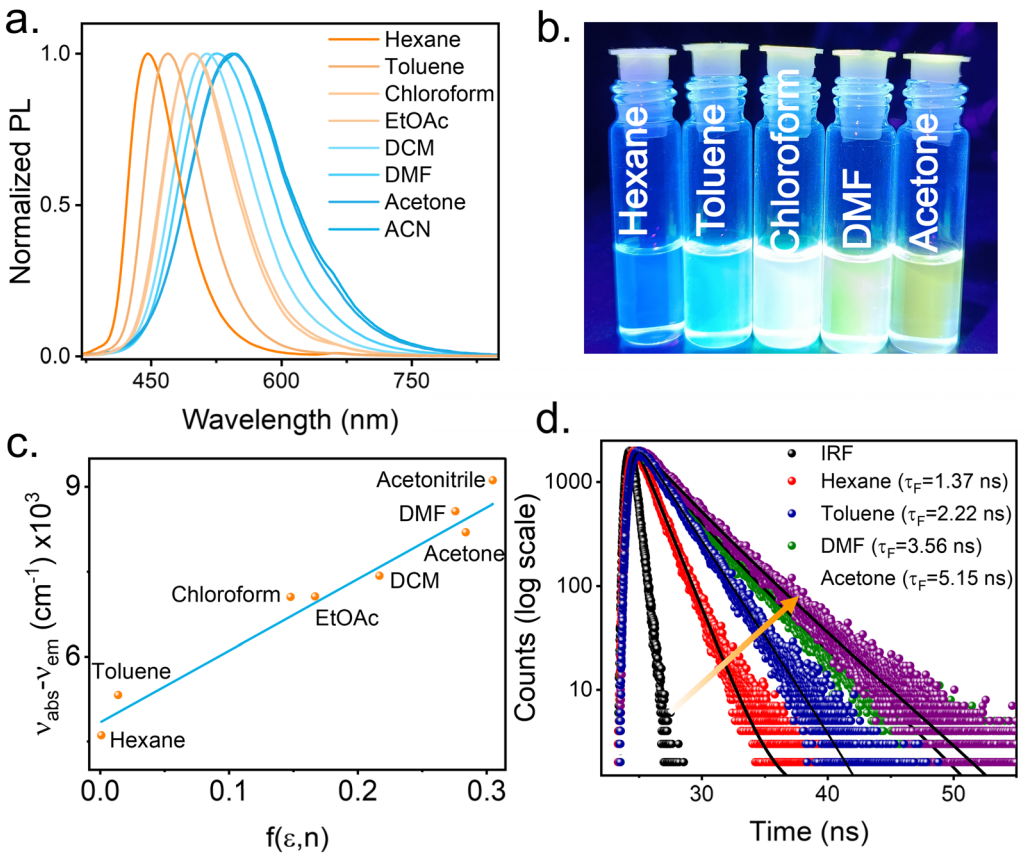

Fig. 3 (a) Normalized PL spectra of **1o** in different solvents and (b) snapshots of **1o** solution in different solvents. (c) Solvatochromic Lippert–Mataga plot for **1o**, showing the linear fit. (d) Variation in fluorescence decay (TCSPC) of **1o** in different organic solvents of different polarity indices.

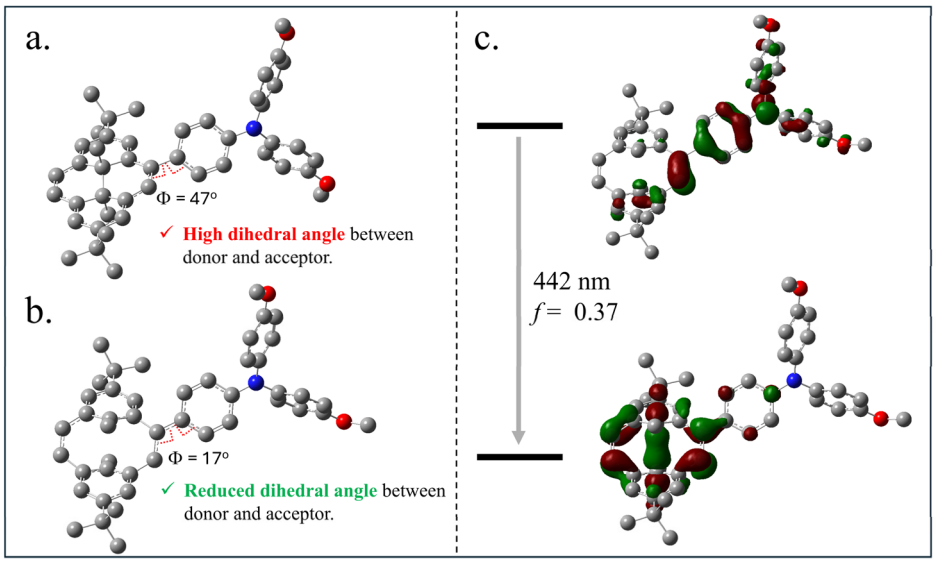

Fig. 4 TD-DFT-optimized first excited-state geometries of **1c** (a) and **1o** (b) at the CAM-B3LYP/6-311G(d) level with PCM (toluene); (c) dominant natural transition orbital (NTO) pair associated with the predicted 442 nm emission, indicating charge-transfer character.

line, Fig. 2b) or by heating (Fig. 2c), thereby promoting the regeneration of the closed isomer (o → c) (Table 2 and Fig. 2c, d). To investigate the nature of this band, we then extended our emission studies in different solvents for **1c** and **1o** isomers. The **1o** isomer showcased a remarkable positive solvatochromism with the emission maxima shifting from 446 nm in hexane to 547 nm in acetonitrile, corresponding to an overall displacement of 101 nm with a visible change in colour (Fig. 3a and b). This solvatochromic nature of the emission band can easily be understood by an intramolecular charge transfer in the excited state. To further augment our understanding of the nature of charge transfer of the excited state, we constructed a Lippert–Mataga correlation plot. A clear linear increase was observed upon moving from low polarity to high polarity media, indicating a dominant charge transfer contribution to the emissive state (Fig. 3c and S34 and Table S3). From the time-resolved photoluminescence analysis, we measured delayed PL lifetimes for **1o** in various solvents. With a gradual increase in the solvent polarity, the fluorescence lifetimes progressively increased from hexane (τ_F = 1.37 ns), toluene (τ_F = 2.22 ns), DMF (τ_F = 3.56 ns), to acetone (τ_F = 5.15 ns) (Fig. 3d and Table S4). This steady increase in lifetime is consistent with the stabilization of a charge transfer excited state in polar media. Compounds **1** and **2** differ in the electron-donating ability of the triarylamine units, with **1** containing a *p*-methoxy unit, which is a relatively strong donor. The closed isomers **1c** and **2c**, respectively, exhibited almost no difference in their fluorescent quantum yield (Φ_{em}, 1.02% (**1c**) *vs.* 1.13% (**2c**)). However, the change is notable in the corresponding open isomers **1o** and **2o** (Φ_{em}, 31.3% (**1o**) *vs.* 6.12% (**2o**)), indicating a role of a charge transfer event, which is much more effective in the presence of a stronger donor unit (Table 2). When the fluorescence emission of the closed isomer **1c** (540 M^{-1} cm^{-1}) was compared to that of **1o** (8800 M^{-1} cm^{-1}), we found an almost 16-fold increase in the brightness. Excited state geometry optimization (TD-DFT, CAM-B3LYP/6-311g(d)) revealed a pronounced conformational difference between the closed and open isomers. In the closed form **1c**, the interplanar dihedral angle between the triphenylamine donor and the DHP unit is approximately ~47°, indicating weak electronic coupling. Ring opening to **1o** reduces this angle to about ~17°, enhancing planarity and enabling efficient charge transfer, consistent with the appearance of a new CT band (Fig. 4a and b and see Table S5 for the remaining derivatives). To further substantiate the charge-transfer assignment, the lowest-energy emissive states were analyzed using TD-DFT with the long-range-corrected CAM-B3LYP functional, the 6-311G(d) basis set, and PCM (toluene) (see the SI for computational details). The lowest emissive transition of **1o** is predicted at 442 nm with substantial oscillator strength (f = 0.37) and pronounced donor-to-acceptor character from the triphenylamine unit to the DHP core, as further supported by natural transition orbital (NTO) analysis, in which the dominant hole–particle pair (Fig. 4c) accounts for ~67% of the total transition character, whereas no comparably intense low-energy transition is found for **1c**, with any analogous excitation carrying negligible oscillator strength (f < 0.05), consistent with weak electronic coupling in the closed geometry (Fig. 4c). In addition, the high aromatic stabilization of the dimethyldihydropyrene core in **1c** disfavours charge transfer, as its participation would require loss of aromatic character. In compound **3**, the fluorescent quantum yield for the **3c** isomer (Φ_{em}, 0.85% (**3c**)) is almost on par with **1c** and **2c** but for photoisomer **3o**, a significant drop in the fluorescence (Φ_{em}, 8.38% (**3o**)) intensity has been observed compared to **1o**. This is anticipated because electron donation from both sides weakens the acceptor and, overall, reduces the charge-transfer process. The incorporation of a *p*-benzaldehyde at the opposite side of the triaryl substitution position in compound **4** resulted in

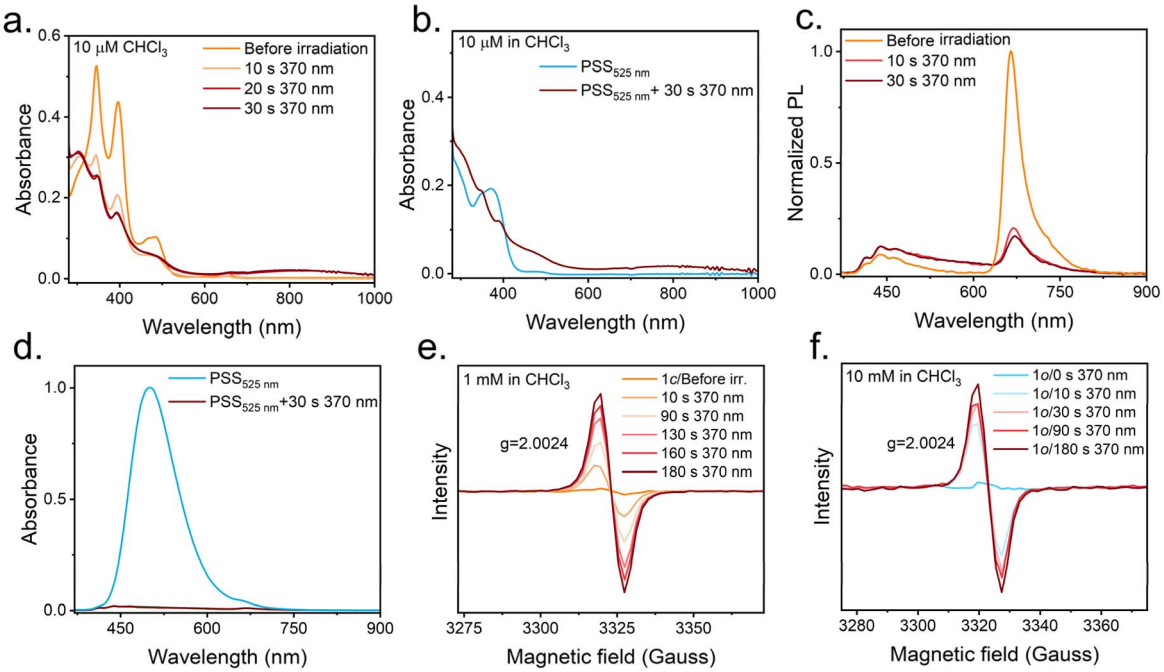

Fig. 5 UV-vis-NIR absorption spectra of (a) **1c** and (b) **1o** and the corresponding PL spectra of (c) **1c** and (d) **1o** under 370 nm light irradiation in 10 μM $CHCl_3$. EPR spectra of (e) **1c** and (f) **1o** under 370 nm light irradiation in 1 mM chloroform solvent.

minimal changes in the absorption and emission spectra of **4c**. However, for the open isomer **4o**, a 15 nm red shift in the emission maximum was observed. The lowering of the fluorescence QY (Φ_{em}, 5.27% (**4o**)) suggests that the electron-withdrawing nature of *p*-benzaldehyde diminishes the CT-induced emission (Table 2). The PL intensity for both isomers of compound **5** is too low to measure the quantum yield error-free (Fig. S16). For completeness, the lowest-energy emissive states were analyzed for all derivatives in both open and closed forms, and the resulting transition energies and oscillator strengths are summarized in Table S6. In each case, the calculated trends in emission energy and relative intensity between the two isomers are in line with the experimentally observed differences. Besides the switching of fluorescence with light, the formation of a stable radical cation species was also observed with the TPA–DHP derivatives upon exposure to light. Substituted triphenylamine (TPA) moieties are well known to generate radical cations. A prime example is magic blue, which is a commercially available TPA-derivative frequently used as a one-electron oxidant.[67] The substituents at the *para* positions are crucial for obtaining stable radicals; otherwise, benzamidine-type reactions can lead to the quenching of the radical cations.[68] Photoinduced radical formation in triphenylamine derivatives has emerged only recently, with only a few reports demonstrating this behavior, mainly in amide-linked derivatives.[53,62,69] At first, when the **1c** isomer of compound **1** was exposed to 370 nm light in $CHCl_3$, a broad absorption band appeared along with a decrease in the intensities of major absorption bands in the UV region, suggesting light-mediated radical generation (Fig. 5a). We wondered whether radical formation occurred only in the ring-closed isomer **1c** under exposure to 370 nm UV light or whether it could also occur with the open isomer **1o**. Thus, we first subjected the sample to 525 nm light, which yielded almost quantitative **1o** isomerization, followed by 370 nm exposure, which also generated a similar broad band in the longer wavelength region centred around 800 nm, suggesting the generation of similar radical species (Fig. 5b). In both cases, a significant decrease in the PL intensity was observed (Fig. 5c and d). We further confirmed the 370 nm light-induced radical formation by EPR measurements. As expected, before irradiation, neither isomer **1c** nor **1o** showed any signal; however, upon irradiation with 370 nm light, a broad signal with $g = 2.0024$ began to appear in both cases (Fig. 5e and f). The photoinduced generation of radical cations was investigated by ^{1}H NMR spectroscopy. When we exposed a $CDCl_3$ solution of isomer **1c** with 370 nm light for 180 seconds, the signals corresponding to the central photochromic DHP moiety broadened (Fig. 6a) before finally generating a species that could not be locked in the NMR instrument. This observation suggests that the unpaired electron density in $\mathbf{1c}^{\bullet+}$ is delocalised over the photochromic DHP unit. To further substantiate this interpretation, the spin-density distribution of $\mathbf{1c}^{\bullet+}$ was computed in $CHCl_3$ using a PCM solvation model, indicating pronounced delocalization of the unpaired electron across the photochromic DHP framework (Fig. 6b). The formation of radicals upon light irradiation was consistently detected across all derivatives. In chloroform, the appearance of a broad EPR resonance provided clear evidence for the generation of paramagnetic species (Fig. S38). The mechanism of photoinduced radical cation generation involves one-electron transfer from the TPA unit of the DHP–TPA to chloroform, followed by the

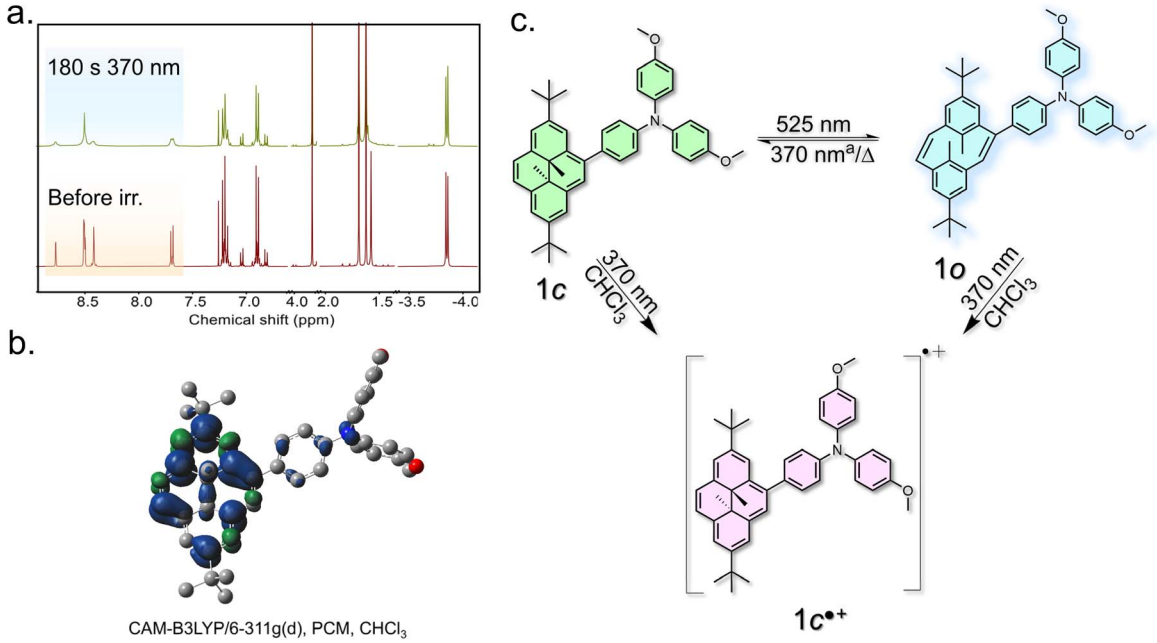

Fig. 6 (a) ^{1}H NMR of **1c** (10 mM $CDCl_3$) before irradiation and after irradiation with 370 nm wavelength light. (b) The spin density distribution map of **1c** in $CHCl_3$, showing that the spin density is distributed over the DHP scaffold. (c) Schematic representing the bifunctional behaviour of the system; [a]in non-chlorinated solvents.

electron donation of the DHP to the TPA moiety, resulting in the formation of the DHP-based radical cation, $[DHP–TPA]^{\bullet+}$.[53] Next, as a control study, we have examined whether photoinduced radical cation formation occurs in other non-chlorinated solvents, namely, toluene, THF, acetonitrile, DMF, methanol, acetone and DMSO. Interestingly, in none of the solvents, the characteristic broad absorption bands in the longer-wavelength region, indicating the formation of the radical species, were observed (Fig. S36). All the samples in these solvents were EPR silent as well. However, the radical cation can be generated even in a non-chlorinated solvent, such as acetonitrile, by chemical oxidation (Fig. S37).

It is crucial to emphasize that as previously discussed in this work, the ring closing (o → c) isomerization can also be triggered by 370 nm light. Therefore, it is difficult to figure out whether **1o** itself generates radical cations to give $\mathbf{1o}^{\bullet+}$ (option A, see below) or, first, isomerizes to **1c** (**1o** → **1c**), and then generates $\mathbf{1c}^{\bullet+}$, *i.e.*, option B.

o → o radical species (option A), or

o → c → c radical species (option B)

Thus, we conducted a control experiment where we compared the photogenerated $\mathbf{1c}^{\bullet+}$ and $\mathbf{1o}^{\bullet+}$ with the same species generated chemically by using an oxidant.[70] Thus, the radical cations, $\mathbf{1c}^{\bullet+}$ and $\mathbf{1o}^{\bullet+}$ were generated chemically by oxidizing them with $Cu(ClO_4)_2$. Subsequently, the UV-vis absorption profiles of $\mathbf{1c}^{\bullet+}$ and $\mathbf{1o}^{\bullet+}$ generated in the chemical and photochemical methods were compared (Fig. 5a, b and S35). For **1c**, both photoinduced and chemically generated $\mathbf{1c}^{\bullet+}$ spectra matched well, but for **1o**, chemically generated $\mathbf{1o}^{\bullet+}$ absorption spectra showed a clearly different signature. If we look closely, the absorption spectrum generated by 370 nm light closely resembles the spectrum of the $\mathbf{1c}^{\bullet+}$ radical cation; a faint presence of the 336 nm and 398 nm bands and a broad band around ~470 nm (absent in chemically generated $\mathbf{1o}^{\bullet+}$) are visible in both cases. This substantiates that both isomers **1c** and **1o**, upon irradiation with 370 nm light, generate $\mathbf{1c}^{\bullet+}$. Next, the stability of the photogenerated radical cations has been evaluated. After generating the radical cation by irradiation with 370 nm light for 180 seconds, the EPR signal intensity was monitored over time. Except for compound **2**, the derivatives exhibited substantial stability, retaining detectable paramagnetic character even after 24 hours. In contrast, compound **2** displayed markedly reduced stability; after 24 h, the EPR signal completely flattened. This can be attributed to the unsubstituted para positions of the triphenylamine unit, where the radical cation species is susceptible to dimerization through a benzamidine-type intermediate, as discussed previously (Fig. S39).

Conclusions

In summary, this work establishes a new paradigm for "turn-on" fluorescence switching within a negative photochromic DHP framework. This was accompanied by the formation of a radical species (Fig. 6c). The reversible change in aromatic character governs the emergence of a charge transfer pathway, which in turn dictates the intensity of the emissive response. Notably, the bright fluorescent state is accessed using visible

light at 525 nm, a wavelength that is compatible with biological environments and practical optical applications. The origin of the charge transfer band is rationalized through detailed theoretical analysis, providing a molecular-level insight into the switching mechanism. Beyond fluorescence control, the same molecular architecture in the closed isomer enables the formation of a stable radical cation under well-defined conditions. This dual fluorescence-radical functionality highlights the power of molecular design in integrating multiple photochemical responses within a single system. Such behavior moves beyond isolated sensing or imaging and points toward unified platforms capable of performing both roles simultaneously. The high-emission state is well suited for super-resolution imaging strategies that rely on controlled fluorescence modulation. At the same time, the generation of stable organic radical cations introduces opportunities in therapeutic or antimicrobial contexts, given the known biological activity of radical species. Collectively, this study demonstrates that multifunctional photoresponsive systems combining emission control and radical chemistry are both achievable and highly promising for future applications.

Author contributions

S. Molla performed synthesis, photophysical studies and analysis, writing, and editing. S. Mahato performed the theoretical investigation, writing and editing. A. K. R. performed the photophysical studies and analysis. S. B. conceptualized the work, acquired funding, provided the resources, and wrote and edited the manuscript. All authors have approved the final version of the manuscript.

Conflicts of interest

There are no conflicts to declare.

Data availability

CCDC 2507057 and 2507332 contain the supplementary crystallographic data for this paper.[71a,b]

The data supporting this article have been included as part of the supplementary information (SI). Supplementary information: NMR spectra, single crystal X-ray structures, and further experimental details. See DOI: https://doi.org/10.1039/d6sc01682k.

Acknowledgements

The authors acknowledge support from DST-SERB (grant SERB CRG/2022/006776) to S. B. The doctoral fellowship provided by CSIR-India to S. Molla is gratefully acknowledged. S. Mahato is supported by a fellowship from NSERC and MITACS, Canada. S. Mahato thanks Dr Tim Storr and the Digital Research Alliance of Canada. A. K. R. is supported by a UGC fellowship. The authors acknowledge Sk Samsul Ghaus for his assistance with TCSPC.

References

1 A. Martin and P. Rivera-Fuentes, *Nat. Chem.*, 2024, **16**, 28–35.
2 B. Wang, H. Cai, G. I. N. Waterhouse, X. Qu, B. Yang and S. Lu, *Small Sci.*, 2022, **2**, 2200012.
3 J. M. Ha, S. H. Hur, A. Pathak, J. E. Jeong and H. Y. Woo, *NPG Asia Mater.*, 2021, **13**, 53.
4 E. Betzig, G. H. Patterson, R. Sougrat, O. W. Lindwasser, S. Olenych, J. S. Bonifacino, M. W. Davidson, J. Lippincott-Schwartz and H. F. Hess, *Science*, 2006, **313**, 1642–1645.
5 S. Adak, S. A. Rahaman, S. Karmakar and S. Bandyopadhyay, *Chem.–Asian J.*, 2024, **19**, e202400400.
6 F. Würthner and M. Hariharan, *Trends Chem.*, 2025, **7**, 208–224.
7 V. B. Patil, D. D. Ugale, S. V. Bhosale and S. V. Bhosale, *Aggregation-induced Emiss. Luminogens Sens. Appl.*, 2025, pp. 102–116.
8 X. Wang, Q. Ding, R. R. Groleau, L. Wu, Y. Mao, F. Che, O. Kotova, E. M. Scanlan, S. E. Lewis, P. Li, B. Tang, T. D. James and T. Gunnlaugsson, *Chem. Rev.*, 2024, **124**, 7106–7164.
9 T. Grotjohann, I. Testa, M. Leutenegger, H. Bock, N. T. Urban, F. Lavoie-Cardinal, K. I. Willig, C. Eggeling, S. Jakobs and S. W. Hell, *Nature*, 2011, **478**, 204–208.
10 H. Li and J. C. Vaughan, *Chem. Rev.*, 2018, **118**, 9412–9454.
11 Q. Qi, C. Li, X. Liu, S. Jiang, Z. Xu, R. Lee, M. Zhu, B. Xu and W. Tian, *J. Am. Chem. Soc.*, 2017, **139**, 16036–16039.
12 T. Chen, B. Dong, K. Chen, F. Zhao, X. Cheng, C. Ma, S. Lee, P. Zhang, S. H. Kang, J. W. Ha, W. Xu and N. Fang, *Chem. Rev.*, 2017, **117**, 7510–7537.
13 M. Olesińska-Mönch and C. Deo, *Chem. Commun.*, 2023, **59**, 660–669.
14 Z. X. Han, J. Xiong, T. B. Ren and X. B. Zhang, *Chem.–Asian J.*, 2022, **17**, e202200387.
15 J. Li, X. Ma, Y. Wang, Y. Cheng, Y. Qin, J. Zhai and X. Xie, *Anal. Chem.*, 2023, **95**, 11664–11671.
16 Q. Qi, Y. Liu, V. Puranik, S. Patra, Z. Svindrych, X. Gong, Z. She, Y. Zhang and I. Aprahamian, *J. Am. Chem. Soc.*, 2025, **147**, 16404–16411.
17 J. Bu, K. Watanabe, H. Hayasaka and K. Akagi, *Nat. Commun.*, 2014, **5**, 3799.
18 J. Zhang, Y. Fu, H. H. Han, Y. Zang, J. Li, X. P. He, B. L. Feringa and H. Tian, *Nat. Commun.*, 2017, **8**, 987.
19 K. Mutoh, N. Miyashita, K. Arai and J. Abe, *J. Am. Chem. Soc.*, 2019, **141**, 5650–5654.
20 A. Eklund, S. Hu, Y. Fang, H. Savolainen, H. Pi, H. Zeng, A. Priimagi, O. Ikkala and H. Zhang, *Adv. Opt. Mater.*, 2024, **12**, 2302487.
21 B. Roubinet, M. Weber, H. Shojaei, M. Bates, M. L. Bossi, V. N. Belov, M. Irie and S. W. Hell, *J. Am. Chem. Soc.*, 2017, **139**, 6611–6620.
22 S. W. Hell, *Nat. Biotechnol.*, 2003, **21**, 1347–1355.
23 K. Uno, M. L. Bossi, M. Irie, V. N. Belov and S. W. Hell, *J. Am. Chem. Soc.*, 2019, **141**, 16471–16478.
24 J. Cusido, E. Deniz and F. M. Raymo, *Eur. J. Org. Chem.*, 2009, 2031–2045.

25 F. V. Subach, L. Zhang, T. W. J. Gadella, N. G. Gurskaya, K. A. Lukyanov and V. V. Verkhusha, *Chem. Biol.*, 2010, **17**, 745–755.
26 H. Chen, Z. Tang, Y. Yang, Y. Hao and W. Chen, *Molecules*, 2024, **29**, 2521.
27 R. Métivier, S. Badré, R. Méallet-Renault, P. Yu, R. B. Pansu and K. Nakatani, *J. Phys. Chem. C*, 2009, **113**, 11916–11926.
28 E. Deniz, M. Tomasulo, J. Cusido, S. Sortino and F. M. Raymo, *Langmuir*, 2011, **27**, 11773–11783.
29 J. Su, T. Fukaminato, J. Placial, T. Onodera, R. Suzuki, H. Oikawa, A. Brosseau, F. Brisset, R. Pansu, K. Nakatani and R. Métivier, *Angew. Chem., Int. Ed.*, 2016, **128**, 3726–3730.
30 A. Bodén, D. Ollech, A. G. York, A. Millett-Sikking and I. Testa, *Nat. Methods*, 2024, **21**, 882–888.
31 M. J. Rust, M. Bates and X. Zhuang, *Nat. Methods*, 2006, **3**, 793–795.
32 T. Kawai, T. Sasaki and M. Irie, *Chem. Commun.*, 2001, 711–712.
33 E. Deniz, S. Sortino and F. M. Raymo, *J. Phys. Chem. Lett.*, 2010, **1**, 1690–1693.
34 A. A. Beharry and G. A. Woolley, *Chem. Soc. Rev.*, 2011, **40**, 4422–4437.
35 R. Klajn, *Chem. Soc. Rev.*, 2014, **43**, 148–184.
36 S. Kar, S. Mahato, S. Chatterjee, S. Molla and S. Bandyopadhyay, *ACS Appl. Opt. Mater.*, 2025, **3**, 2960–2970.
37 M. Herder, B. M. Schmidt, L. Grubert, M. Pätzel, J. Schwarz and S. Hecht, *J. Am. Chem. Soc.*, 2015, **137**, 2738–2747.
38 J. Wu, L. Kreimendahl and J. L. Greenfield, *Angew. Chem., Int. Ed.*, 2025, **64**, e202415464.
39 M. Larkowska, M. Wuebbenhorst and S. Kucharski, *Int. J. Polym. Sci.*, 2011, 627195.
40 Y. Funasako, H. Miyazaki, T. Sasaki, K. Goshima and M. Inokuchi, *J. Phys. Chem. B*, 2020, **124**, 7251–7257.
41 S. Hatano, T. Horino, A. Tokita, T. Oshima and J. Abe, *J. Am. Chem. Soc.*, 2013, **135**, 3164–3172.
42 S. Helmy, S. Oh, F. A. Leibfarth, C. J. Hawker and J. Read De Alaniz, *J. Org. Chem.*, 2014, **79**, 11316–11329.
43 K. Klaue, W. Han, P. Liesfeld, F. Berger, Y. Garmshausen and S. Hecht, *J. Am. Chem. Soc.*, 2020, **142**, 11857–11864.
44 S. Molla, J. Ahmed and S. Bandyopadhyay, *Chem. Sci.*, 2025, **16**, 13694–13703.
45 S. Molla and S. Bandyopadhyay, *J. Mater. Chem. C*, 2024, **12**, 17511–17518.
46 S. Aiken, R. J. L. Edgar, C. D. Gabbutt, B. M. Heron and P. A. Hobson, *Dyes Pigm.*, 2018, **149**, 92–121.
47 C. B. McArdle, H. Blair, A. Barraud and A. Ruaudel-Teixier, *Langmuir–Blodgett Film, 1982*, 1983, pp. 181–188.
48 J. Ahmed, S. Ghosh, S. Chatterjee, S. Molla and S. Bandyopadhyay, *Chem.–Eur. J.*, 2025, **31**, e02649.
49 Z. X. Chen, Y. Li and F. Huang, *Chem*, 2021, **7**, 288–332.
50 T. Kubo and M. Abe, *Chem. Rev.*, 2024, **124**, 4541–4542.
51 J. Xu, S. Li, Y. Yang and Z. Chen, *Chem.–Eur. J.*, 2023, **29**, e202203598.
52 S. Kimura, A. Tanushi, T. Kusamoto, S. Kochi, T. Sato and H. Nishihara, *Chem. Sci.*, 2018, **9**, 1996–2007.
53 X. Rong, J. Liu, J. Wu, C. Li, K. Wang, Z. Lu, Y. Liu, M. Gu and Y. Huang, *J. Mater. Chem. C*, 2023, **11**, 9640–9648.
54 K. P. Rao, T. Kusamoto, F. Toshimitsu, K. Inayoshi, S. Kume, R. Sakamoto and H. Nishihara, *J. Am. Chem. Soc.*, 2010, **132**, 12472–12479.
55 L. Mao, M. Zhou, X. Shi and H. B. Yang, *Chin. Chem. Lett.*, 2021, **32**, 3331–3341.
56 H. Cao, T. Li, L. Zhao, Y. Qiang, X. Zheng, S. Dai, Y. Chen, Y. Zhu, L. Zhao, R. Cai, Z. Sun, F. Li, Y. Yang, L. Zhang, H. L. Yip and Z. Yu, *ACS Energy Lett.*, 2025, **10**, 2017–2025.
57 A. Farokhi, H. Shahroosvand, G. D. Monache, M. Pilkington and M. K. Nazeeruddin, *Chem. Soc. Rev.*, 2022, **51**, 5974–6064.
58 W. Z. Gao, X. G. Li, S. R. Wang and H. J. Lv, *Chin. Chem. Lett.*, 2012, **23**, 141–144.
59 K. Sreenath, C. V. Suneesh, V. K. Ratheesh Kumar and K. R. Gopidas, *J. Org. Chem.*, 2008, **73**, 3245–3251.
60 A. M. Thangthong, N. Prachumrak, R. Tarsang, T. Keawin, S. Jungsuttiwong, T. Sudyoadsuk and V. Promarak, *J. Mater. Chem.*, 2012, **22**, 6869–6877.
61 J. Hu, J. Wang, T. H. Nguyen and N. Zheng, *Beilstein J. Org. Chem.*, 2013, **9**, 1977–2001.
62 A. J. Sindt, B. A. Dehaven, D. F. McEachern, D. M. M. M. Dissanayake, M. D. Smith, A. K. Vannucci and L. S. Shimizu, *Chem. Sci.*, 2019, **10**, 2670–2677.
63 A. J. Sindt, B. A. Dehaven, D. W. Goodlett, J. O. Hartel, P. J. Ayare, Y. Du, M. D. Smith, A. K. Mehta, A. M. Brugh, M. D. E. Forbes, C. R. Bowers, A. K. Vannucci and L. S. Shimizu, *J. Am. Chem. Soc.*, 2020, **142**, 502–511.
64 P. Ravat, T. Šolomek, D. Häussinger, O. Blacque and M. Juríček, *J. Am. Chem. Soc.*, 2018, **140**, 10839–10847.
65 P. Jana, S. Koppayithodi, S. Mahato, S. Molla and S. Bandyopadhyay, *J. Phys. Chem. Lett.*, 2023, **14**, 7433–7439.
66 J. Schlecht, T. Lohmiller, P. Thielert, C. Douglas, M. Gather, S. Richert and O. Dumele, *Angew. Chem., Int. Ed.*, 2025, **64**, e202515144.
67 A. I. Hofmann, R. Kroon, S. Zokaei, E. Järsvall, C. Malacrida, S. Ludwigs, T. Biskup and C. Müller, *Adv. Electron. Mater.*, 2020, **6**, 2000249.
68 M. Roy, J. H. Walton, J. C. Fettinger and A. L. Balch, *Chem.–Eur. J.*, 2022, **28**, e202104631.
69 G. I. P. Wijesekera, F. A. Gbadamosi, M. S. Hossain, A. Patra, C. Sutton and L. S. Shimizu, *J. Phys. Chem. C*, 2024, **128**, 16713–16720.
70 K. Sreenath, T. G. Thomas and K. R. Gopidas, *Org. Lett.*, 2011, **13**, 1134–1137.
71 (*a*) CCDC 2507057: Experimental Crystal Structure Determination, 2026, DOI: 10.5517/ccdc.csd.cc2q4sth; (*b*) CCDC 2507332: Experimental Crystal Structure Determination, 2026, DOI: 10.5517/ccdc.csd.cc2q52pp.